International Journal of Biological Macromolecules 146 (2020) 363–373

Contents lists available at ScienceDirect

International Journal of Biological Macromolecules

journal homepage: http://www.elsevier.com/locate/ijbiomac

Host-guest fabrication of dual-responsive hyaluronic acid/mesoporous silica nanoparticle based drug delivery system for targeted cancer therapy

Jinbo Lu [a,b,1], Bichu Luo [a,b,1], Zhongyin Chen [a], Ye Yuan [b], Ying Kuang [c], Lihui Wan [a], Li Yao [a], Xueqin Chen [a], Bingbing Jiang [a], Jia Liu [b,*], Cao Li [a,*]

[a] Ministry-of-Education Key Laboratory for the Green Preparation and Application of Functional Materials, Hubei Key Laboratory of Polymer Materials, Hubei University, Wuhan 430062, China
[b] Research Center for Tissue Engineering and Regenerative Medicine, Union Hospital, Tongji Medical College, Huazhong University of Science and Technology, Wuhan 430022, China
[c] Glyn O. Philips Hydrocolloid Research Centre at HUT, Hubei University of Technology, Wuhan 430068, China

ARTICLE INFO

Article history:
Received 13 June 2019
Received in revised form 22 November 2019
Accepted 31 December 2019
Available online 03 January 2020

Keywords:
Targeted cancer therapy
pH/redox-dual-responsive
Mesoporous silica nanoparticle

ABSTRACT

In this paper, a targeting hyaluronic acid (HA)/mesoporous silica nanoparticle (MSN) based drug delivery system (DDS) with dual-responsiveness was prepared for cancer therapy. To avoid the side reaction between the anti-cancer drug doxorubicin hydrochloride (DOX) and HA, host-guest interaction was applied to fabricate the DDS named DOX@MSN-SS-N=C-HA. The "nanocontainer" MSN was modified with benzene ring *via* both pH-sensitive benzoic imine bond and redox-sensitive disulfide linkage. When DOX was loaded in the pores of MSN, the channels were then capped by the "gatekeeper" β-CD grafted HA (HA-*g*-CD) through host-guest interaction between β-CD and benzene. HA endowed the drug carriers with the targeting capability in CD44 over-expressed cancer cells. After cellular uptake, the carriers could rapidly release DOX for cell apoptosis due to both the hydrolysis of benzoic imine bond at low pH and the cleavage of disulfide bond at a high concentration of glutathione (GSH) intracellular. *In vitro* drug release studies and *in vitro* cytotoxicity studies were taken to investigate the dual-responsiveness of the carriers. And the CD44-receptor mediated cancer cell targeting capability was investigated as well. In conclusion, the targeted dual-responsive complex DDS fabricated through host-guest interaction has promising potential in cancer therapy.

1. Introduction

Chemotherapy remains one of the major therapeutic approaches applied to treat cancer in clinic. However, the disadvantages of traditional chemotherapeutic drugs such as unfavorable pharmacokinetics, poor biodistribution and lack of selectivity for target tissues reduce the utilization of the drugs and cause serious side effects [1]. To tackle these problems, anti-cancer drug delivery systems (DDSs) based on nanotechnology have been introduced and developed rapidly in recent decades [1–4]. DDSs such as liposomal daunorubicin (DaunoXome), pegylated liposomal doxorubicin (Doxil), albumin nanoparticle based Nan-paclitaxel (Abraxane) and polymeric micelle paclitaxel (Genexol-PM) have already been approved for clinical treatment of cancer [3,4]. These nanosized DDSs can be accumulated in tumor tissues more easily *via* enhanced permeability and retention (EPR) effect to improve the pharmacokinetics and biodistribution of the drugs, as well as to reduce their side effects [5].

Though the commercial DDSs represented by the liposomal doxorubicin can overcome part of the shortcomings of traditional anti-cancer drugs, they cannot or only modestly improve patients' overall survival [3,6–9]. Therefore, more efforts are needed to develop novel advanced DDSs. The properties including controlled drug release based on stimuli- sensitivity [10,11] and ligand-mediated active cancer targeting [12–15] introduced make the newly reported DDSs with better therapeutic effects [1–4]. During the past decade, mesoporous silica nanoparticle (MSN) based DDSs have attracted considerable attention from scientists worldwide [16,17]. MSNs can be simply synthesized with tunable size, shape, pore size and volume [17,18], and are easy surface functionalization [16]. These advantages, as well as the high drug loading capacity and good biocompatibility, ensure that MSNs are excellent choices for designing safe and efficient drug carriers [16–18].

Of course, for pure MSNs, it is difficult to bring and release most of the drugs inside cancer cells with negligible drug losses. Therefore, suitable functional "gatekeepers" are needed [16,19]. A good "gatekeeper"

* Corresponding authors.
E-mail addresses: jialiu1207@hust.edu.cn (J. Liu), licao0415@163.com (C. Li).
[1] J. Lu and B. Luo contributed equally to this work.

https://doi.org/10.1016/j.ijbiomac.2019.12.265
0141-8130/

should plug the channels of MSN effectively to prevent premature drug release until achieving at the right place [19], and; after that the "gatekeeper" should degrade or leave from the carrier due to the change of pH [20–22], temperature [22–24], redox state [24–26], concentration of enzyme [27,28], light [29], *etc.* for controlled drug release [19]. Moreover, besides the controlled release behavior, the "gatekeepers" should endow the DDSs with other features, for instance, tumor targeting capability and synergistic antitumor effect [19,30,31]. For example, Zhang and co-workers applied ZnO Quantum Dots (QDs) as the "gatekeeper" to fabricate a pH-responsive multifunctional MSN based DDS [30]. The obtained ZnO@MSN DDS could achieve a "zero-premature" drug release under a physiological environment but could release the loaded drug in acidic endosome due to the rapid dissolution of ZnO QDs, which could also achieve a synergistic antitumor effect [30]. Chen et al. used the folic acid (FA) modified chitosan (CHI) as the "gatekeeper" to block the pores of MSN *via* both pH and redox dual-sensitive bonds [31]. Due to the FA modification, the drug carriers were active cancer targeting; and the CHI could leave the carriers to release drugs intracellular owing to the low pH and high concentration of reduced glutathione (GSH) [31].

In this paper, MCM-41-type MSN with a size of ~140 nm was utilized to fabricate a cancer targeting dual-responsive DDS with modified hyaluronic acid (HA) as the "gatekeeper". HA is a non-sulfated anionic polysaccharide composed of repeating disaccharide units of D-glucuronic acid (GlcA) and *N*-acetyl-D-glucosamine (GlcNAc) [32,33]. Owing to its excellent biocompatibility, biodegradability and nonimmunogenicity, HA and modified HA are widely researched in biomedical fields [32–34]. More importantly, HA is a targeted ligand of CD44 that is over-expressed in various kinds of cancer cells [32–42]. Therefore, HA has also been introduced as the "gatekeeper" to fabricate MSN based cancer targeting DDSs in recent years [35–42]. However, in most cases, HA was capped on MSNs through an EDC/NHS method based on $-NH_2$ modified on the surface of MSNs and –COOH of HA [35–42]. As the frequently-used anti-cancer drugs such as doxorubicin hydrochloride (DOX) may also react with these functional groups, the reaction between MSN and HA should be noticed. As a result, herein the cyclodextrin (CD) based host-guest interaction was utilized. HA was firstly grafted with β-CD to obtain HA-*g*-CD, and was then capped on the benzaldehyde functionalized MSN *via* host-guest interaction between β-CD and benzene ring. The pH in endosome and lysosome intracellular is lower (4.0–6.0) than that in blood circulation system and normal tissues (~7.4) [43,44]; and the concentration of GSH is much higher in intracellular fluids (up to 10 mM) than that in extracellular fluids (*ca.* 2 μM) [45,46]. Therefore, the benzene ring was modified on MSN through both pH-sensitive benzoic imine bond and redox-sensitive disulfide bond. Based on the design mentioned above, the obtained DDS named DOX@MSN-SS-N=C-HA efficiently transported DOX molecules into CD44 over-expressed cancer cells targeted and quickly unloaded then in response to the intracellular acidity and GSH for killing cancer cells. It is expected the novel DDS could be a valuable choice for cancer therapy.

2. Experimental section

2.1. Chemicals

Sodium hydroxide (NaOH), *N*-cetyltrimethylammonium bromide (CTAB), tetraethyl orthosilicate (TEOS), β-cyclodextrin (β-CD), hydrochloric acid (HCl), diethyl ether, acetic acid, acetone, anhydrous methanol, 4-toluenesulfonyl chloride (*p*-TsCl), ammonia chloride (NH_4Cl) and ethylenediamine (EDA) were purchased from Shanghai Reagent Chemical Co. (Shanghai, China). Benzaldehyde, 2,2′-dithiodipyridine, cysteamine hydrochloride, 3-mercaptopropyltrimethoxysilane (MPTMS), doxorubicin hydrochloride (DOX), 1-ethyl-3-(3-dimethyllamanopropyl) carbodiimide hydrochloride (EDC·HCl), *N*-hydroxysuccinimide (NHS), fluorescein isothiocyanate isomer I (FITC), glutathione (GSH) and L-buthionine-sulfoximine (BSO) were purchased from Aladdin Reagent Co. Ltd. (Shanghai, China). Hyaluronic acid (HA; M_W = 3–10 kDa) was purchased from Bloomage Freda Biopharm Co. Ltd. (Jinan, China). Dulbecco's modified eagle medium (DMEM), Roswell Park Memorial Institute (RPMI) 1640 medium, fetal bovine serum (FBS), 3-[4,5-dimethylthiazol-2-yl]-2,5-diphenyltetrazolium-bromide (MTT), phosphate buffered saline (PBS) and 4′,6-diamidino-2-phenylindole (DAPI) were purchased from Invitrogen Co (America). All reagents were of analytical grade and were used without further treatment or purification. 6-EDA-β-cyclodextrin (β-CD-NH_2) [47] and *S*-(2-aminoethylthio)-2-thiopyridine hydrochloride [48] were synthesized according to the reported procedures.

2.2. Synthesis of β-CD grafted hyaluronic acid (HA-g-CD)

500 mg of HA was dissolved in 30 mL of deionized (DI) water. Then 379.4 mg of EDC·HCl and 227.8 mg of NHS were added to the solution, whose pH was adjusted to 5.0. The solution was stirred at 4 °C overnight. After that, 3.0 g of β-CD-NH_2 was added and the solution was stirred at room temperature for 48 h. After reaction, the solution was dialyzed (MWCO: 3500 Da) against DI water for 6 days and then lyophilized to obtain HA-*g*-CD.

2.3. Preparation of 3-mercaptopropyl-functionalized MSN (MSN-SH)

MSN-SH was prepared following a literature procedure [49]. 1.0 g of CTAB and 0.8 g of NaOH was dissolved in 480 mL of DI water. The solution was heated to 80 °C under vigorous stirring. After that, 5.0 mL of TEOS and 0.97 mL of MPTMS were added dropwise to the solution in sequence. Then the reaction was taken at 80 °C under vigorous stirring for another 2 h. After being cooled to room temperature, the white solid was collected from the reaction mixture through centrifugation (9500 r/min × 10 min). The precipitate was washed with abundant methanol and DI water and was then lyophilized to obtain the CTAB contained MSN-SH (CTAB@MSN-SH). To remove the surfactants, 1.0 g of CTAB@MSN-SH was dispersed in 160 mL of anhydrous methanol containing 9.0 mL of HCl (37%). The mixture was refluxed at 60 °C for 48 h, followed by extensive washing with methanol and DI water. The washed sample was lyophilized to obtain MSN-SH.

2.4. Preparation of 2-(propyldisulfanyl)ethylamine functionalized MSN (MSN-SS-NH_2)

800 mg of MSN-SH was suspended in 160 mL of methanol. Then, 800 mg of *S*-(2-aminoethylthio)-2-thiopyridine hydrochloride was added to the mixture. The reaction was taken at room temperature under vigorous stirring for 24 h. The product was centrifuged, washed with abundant methanol and DI water, and then lyophilized to give MSN-SS-NH_2.

2.5. Preparation of benzaldehyde functionalized MSN-SS-NH_2 (MSN-SS-N=C-Ph)

500 mg of MSN-SS-NH_2 was suspended in 100 mL of PBS (pH 8.0). Then, 1.5 mL of benzaldehyde was added to the mixture. The reaction was taken at room temperature under vigorous stirring for 24 h. The product was centrifuged, washed with PBS (pH 8.0) for several times and at last washed with DI water, and was then lyophilized to give MSN-SS-N=C-Ph.

2.6. Preparation of DOX loaded HA-g-CD capped MSN-SS-N=C-Ph (DOX@MSN-SS-N=C-HA)

The preparation of DOX@MSN-SS-N=C-HA was based on host-guest interaction. 100 mg of MSN-SS-N=C-Ph was suspended in 30 mL of PBS (pH 8.0). Then, 25 mg of DOX was dissolved in the suspension. The

mixture was stirred vigorously for 24 h. After that, 120 mg of HA-*g*-CD was added to the mixture. And the mixture was stirred vigorously for 24 h in dark. The product was centrifuged, washed with PBS (pH 8.0) for several times and at last washed with DI water, and was then lyophilized to give DOX@MSN-SS-N=C-HA. MSN-SS-N=C-HA without loading of DOX was also prepared in a similar way.

2.7. Characterizations

^{1}H NMR spectra of the samples were obtained using an Inova 600 nuclear magnetic resonance spectrometer (NMR; Varian, USA). The morphology of MSN-SH and DOX@MSN-SS-N=C-HA was observed by a Tecnai G20 transmission electron microscope (TEM; FEI, USA). Small angle X-ray scattering (SAX) was taken with a D8 Discover X-ray diffractometer (Bruker, Germany). Data of particle sizes and zeta-potentials were obtained using a Zetasizer Nano ZS90 analyzer (Malvern, UK). The surface area of the nanoparticles was calculated by the Brunauer–Emmett–Teller (BET) method, and pore volume, as well as pore size, was obtained by the Barrett–Joyner–Halenda (BJH) approach (JW-BK112, Beijing JWGB, China). Fourier transform infrared (FT-IR) spectra of the samples were recorded on a Nicolet iS10 spectrometer (Thermo Fisher, USA). Thermogravimetric analysis (TGA) was performed from 25 °C to 800 °C at a heating rate of 5 °C min^{-1} under N_2 atmosphere with a TGA/DSC 1-1100c analyzer (Mettler Toledo, Sweden). UV–vis spectra were obtained using a Lambda Bio40 UV/vis spectrometer (Perkin-Elmer, USA).

2.8. In vitro drug release studies

Before the *in vitro* drug release studies, the encapsulation efficiency (*EE*) and drug loading capacity (*LC*) of the drug carrier were measured by UV–Vis absorbing after dissolving the nanoparticles in the HF solution, and calculated by the formulas below:

$$EE = \frac{mass\ of\ drug\ loaded\ in\ the\ carriers}{mass\ of\ drug\ fed\ initially} \times 100\%$$

$$LC = \frac{mass\ of\ drug\ loaded\ in\ the\ carriers}{mass\ of\ drug\ loaded\ carriers} \times 100\%$$

The *in vitro* drug release studies were taken at 37 °C in five different buffer solutions: pH 7.4 without GSH, pH 7.4 with 10 mM GSH, pH 6.5 without GSH, pH 5.0 without GHS and pH 5.0 with 10 mM GSH, respectively. For each study, 5.0 mg of DOX@MSN-SS-N=C-HA was suspended in 5.0 mL of buffer solution at indicated condition, which was transferred to a dialysis bag (MWCO: 3500 Da), and then immersed in 35.0 mL of indicated buffer solution immediately. The system was shaken in a water bath at 37 °C. At predetermined time intervals, 4.0 mL of release medium were drawn and replaced with 4.0 mL of fresh medium buffer. The amount of drug released was calculated based on the UV–Vis absorbance of DOX at 493 nm.

2.9. Co-incubation of DOX@MSN-SS-N=C-HA with cells

Murine mammary carcinoma (4T1) and human renal epithelial (293T) cell lines were applied in the studies. The culture mediums for culturing both 4T1 and 293T cells were RPMI-1640 medium and DMEM, respectively. For each study, 4T1 and 293T cells were seeded in a six-well plate at a density of ~1×10^5 cells per well in 1 mL of culture medium with 10% FBS, 100 unit/mL of penicillin and 100 μg/mL of streptomycin, and were incubated at 37 °C under a humidified atmosphere with 5% CO_2 for 24 h. After that, the culture media was removed and replaced with 1 mL of culture media containing DOX@MSN-SS-N=C-HA with a DOX concentration of 4 mg/L. The cells were incubated for a further 4 h. Then the culture medium was removed, and the cells were washed with PBS for three times. After that, the nucleuses were stained with 500 μL of culture medium containing 50 μL of DAPI for 20 min. For the *in vitro* targeting analysis, half of the wells were added with 5 mg/mL HA during the incubation. Finally, the culture medium was removed and the cells were further washed with PBS for several times. Then the cells were observed by a confocal laser scanning microscopy (CLSM, Carl Zeiss LSM 710, Germany).

2.10. Flow cytometry analysis

4T1 and 293T cells were seeded in a six-well plate at a density of ~1×10^5 cells per well in 1 mL of culture medium with 10% FBS, 100 unit/mL of penicillin and 100 μg/mL of streptomycin, and were incubated at 37 °C under a humidified atmosphere with 5% CO_2 for 24 h. After that, the culture media was removed and replaced with 1 mL of culture medium containing DOX@MSN-SS-N=C-HA with a DOX concentration of 4 mg/L. The cells were incubated for a further 4 h. For the *in vitro* targeting analysis, half of the wells were added with 5 mg/mL HA during the incubation. Then the culture medium was removed, and the cells were washed with PBS for three times. All the cells were digested by trypsin and collected in centrifuge tubes by centrifugation (1000 rpm for 5 min). The supernatant was discarded and the bottom cells were washed twice with PBS. Then the suspended cells were filtrated and examined by flow cytometry (Beckman Coulter MoFlo XDP, USA). Cells untreated with nanoparticles were used as a control.

2.11. In vitro cytotoxicity assay

4T1 and 293T cells were seeded in a 96-well plate at a density of ~5.0×10^4 cells per well in 200 μL of culture medium with 10% FBS, 100 unit/mL of penicillin and 100 μg/mL of streptomycin for 24 h to adding blank MSN-SS-N=C-HA (without loading of DOX) at different concentrations. After *co*-incubation with the nanoparticles for 48 h, the culture media were replaced with 200 μL of fresh culture medium and 20 μL of MTT stock solution (5 mg/mL in PBS). The cells were incubated for a further 4 h. After that, the culture medium was removed and 200 μL of DMSO was added. The optical density (OD) at 570 nm was measured using a microplate reader (Model 550, Bio-Rad, USA), and the viability was calculated as:

$$Cell\ viability = \frac{OD_{570(treated)}}{OD_{570(control)}} \times 100\%$$

where $OD_{570(treated)}$ was obtained in the presence of the nanoparticles.

For the cell death assay of DOX loaded DOX@MSN-SS-N=C-HA, the cells were seeded in a 96-well plate in 200 μL of culture medium containing 10% FBS, 100 unit/mL of penicillin and 100 μg/mL of streptomycin. After incubation for 24 h, the culture media was replaced with 200 μL of fresh culture media containing DOX@MSN-SS-N=C-HA or pure DOX at the indicated DOX concentrations. For the *in vitro* targeting analysis, parts of the wells were added with 5 mg/mL HA during the incubation. For 4T1 cells, parts of the wells were added with 20 mM of NH_4Cl, 500 μM of BSO as well as both 20 mM of NH_4Cl and 500 μM of BSO during the incubation, respectively. After *co*-incubation for 48 h, the cell viability was calculated followed by the method mentioned above.

2.12. Statistical analysis

The results of the stability study of DOX@MSN-SS-N=C-HA, *in vitro* release studies, and *in vitro* cytotoxicity were exhibited as mean ± standard deviation (SD) with at least three tests. Statistical significance in difference was analyzed using Student's *t*-test: $^*p < 0.05$, $^{**}p < 0.01$ and $^{***}p < 0.001$.

3. Results and discussion

3.1. Preparation and characterization of the targeting dual-responsive DDS

The "gatekeeper" β-CD grafted HA (HA-*g*-CD) was first synthesized by conjugating β-CD-HN_2 on HA backbone. The ^{1}H NMR spectra of HA, β-CD-HN_2 and HA-*g*-CD are shown in Fig. 1A, B and C respectively, using heavy water as the solvent. For HA, the peaks from ~ 3.0 to 4.2 ppm as well as the two peaks at ~ 4.3–4.6 ppm were attributed to the protons in the sugar rings. The peak at ~2.0 ppm was attributed to the protons in the methyl group. For β-CD-HN_2, as shown in Fig. 1B, the peaks from ~ 2.4 to 2.9 ppm were assigned to the protons in EDA. The peaks from ~ 3.6 to 4.0 ppm and the peak at ~ 5.0 ppm were attributed to the protons in the sugar rings. And the peaks from ~ 3.4 to 3.6 ppm was attributed to the protons of –CH_2– linking the sugar rings and the hydroxyl groups. It is noticed that the entire characteristic peaks of both HA and β-CD-HN_2 appeared in the spectrum of HA-*g*-CD, proved the successful synthesis. By calculating the ratio of the integral area of No. 4 protons' peak of β-CD-HN_2 to No. 12 protons' peak of HA in Fig. 1C, the β-CD modification degree was calculated to be 13% (HA units: β-CD moieties = 10: 1.3) according to the formula below:

$$\beta\text{-}CD\ modification\ degree = \frac{6 \times Integral\ area\ of\ No.4\ protons'peak\ of\ \beta\text{-}CD\text{-}HN_2}{7 \times Integral\ area\ of\ No.12\ protons'peak\ of\ HA} \times 100\%$$

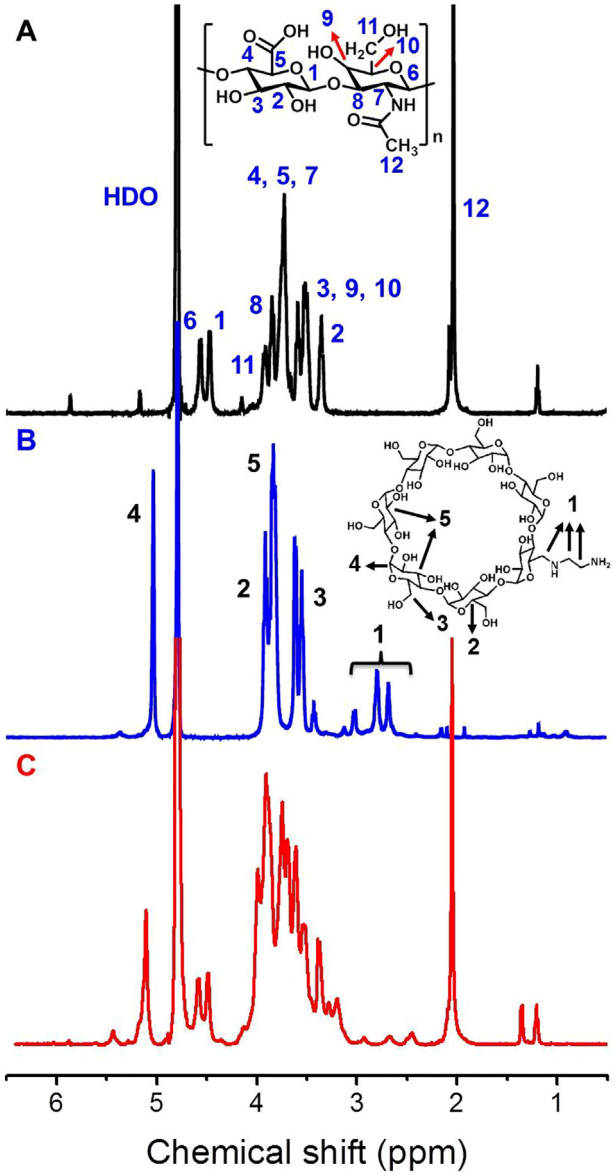

Fig. 1. ^{1}H NMR spectra of HA (A), β-CD-HN_2 (B) and HA-*g*-CD (C).

The "nano-container" MSN-SH was prepared through a sol-gel method. And TEM was applied to visually present the morphological and dimensional characteristics. As shown in Fig. 2A and B, the nanoparticles were uniform spherical shape with highly ordered honeycomb channels at a mesoporous scale. The particle size estimated from the TEM images was ~100 nm, which met the result measured by dynamic light scattering (DLS; 139.4 nm with a PDI of 0.108, Fig. 2D). The N_2 adsorption–desorption isotherms and the pore diameter distribution curves of MSN-SH and modified MSN are shown in Fig. 3. The type IV isotherm curve, as well as the pore diameter distribution, also proved the successful formation of the mesoporous structure of MSN-SH.

As illustrated in Scheme 1, MSN-SH was then surface modified to form MSN-SS-NH_2 with a disulfide bond linking between MSN and amino groups. It is known that zeta-potential, specific surface area, as well as the pore property of mesoporous nanoparticle, should change after the surface modification. Therefore, as listed in Table 1, zeta-potential of MSN-SS-NH_2 was reversed form −28.8 mV of MSN-SH to +41.5 mV because of the positively charged amino group. And the BET surface area (S_{BET}), BJH pore volume (V_p), as well as BJH pore diameter (D_{BJH}), of MSN-SS-NH_2 also reduced from 873 m^2/g, 0.855 cm^3/g and 2.86 nm of MSN-SH to 567 m^2/g, 0.450 cm^3/g and 2.83 nm, respectively. After being modified by benzaldehyde, channels of MSN were further partly blocked. As a result, S_{BET} and V_p of the obtained MSN-SS-N=C-Ph reduced to 323 m^2/g and 0.190 cm^3/g, respectively. And D_{BJH} of the nanoparticles reduced to 2.52 nm as well. Pores of DOX-loaded MSN-SS-N=C-Ph were finally capped with HA-*g*-CD *via* host-guest interaction between β-CD moieties and benzene groups on MSN to form the dual-responsive DOX@MSN-SS-N=C-HA. As shown in Fig. 3A, the isotherm curve of the final carriers was not clear type IV curve anymore. And D_{BJH} of the carriers could not be calculated *via* the pore distribution curve. The results demonstrated that the channels of DOX@MSN-SS-N=C-HA were completely blocked by HA-*g*-CD. And S_{BET} and V_p of the carriers further reduced to 58.0 m^2/g and 0.108 cm^3/g, respectively. Zeta-potentials of MSN-SS-N=C-Ph and DOX@MSN-SS-N=C-HA were −35.8 and −25.3 mV respectively.

The TEM image of DOX@MSN-SS-N=C-HA was also shown in Fig. 2C. It is noticed that the surface of the nanoparticles became rough, and; new even signal appeared on the edge of the nanoparticles. The image proved that HA-*g*-CD had been successfully coated on the surface of the nanoparticles. The particle size of DOX@MSN-SS-N=C-HA measured by DLS was 365.2 nm with a PDI of 0.141 (Fig. 2E). The increase of the particle size may due to the surface modification by HA-*g*-CD as well as the slight aggregation of the nanoparticles during the process of surface modification.

SAX patterns of both MSN-SH and DOX@MSN-SS-N=C-HA are shown in Fig. 2F. Three evidently Bragg peaks assigned as (1 0 0), (1 1 0) and (2 0 0) planes were clearly observed in the pattern of MSN-SH which were consistent with the characteristic diffraction pattern of MCM-41-type MSN. After loading of DOX and surface modification, the diffraction peaks of MSN-SH disappeared in the pattern of DOX@MSN-SS-N=C-HA, proved that after adequately combining with the organic and polymeric components, the pores of MSN-SH had been completely blocked.

The conversion of the nanoparticles' surface was confirmed by FT-IR spectra as well (Fig. 4). In the spectra of the samples, the intense and asymmetric band from ~1080 cm^{-1} can be assigned to the stretching vibration of Si–O–Si; and the band from ~804 cm^{-1} can be assigned to the stretching vibration of Si–OH. As shown in Fig. 4B, MSN-SS-NH_2 exhibited a weak absorption peak at ~1515 cm^{-1}, which was regarded as

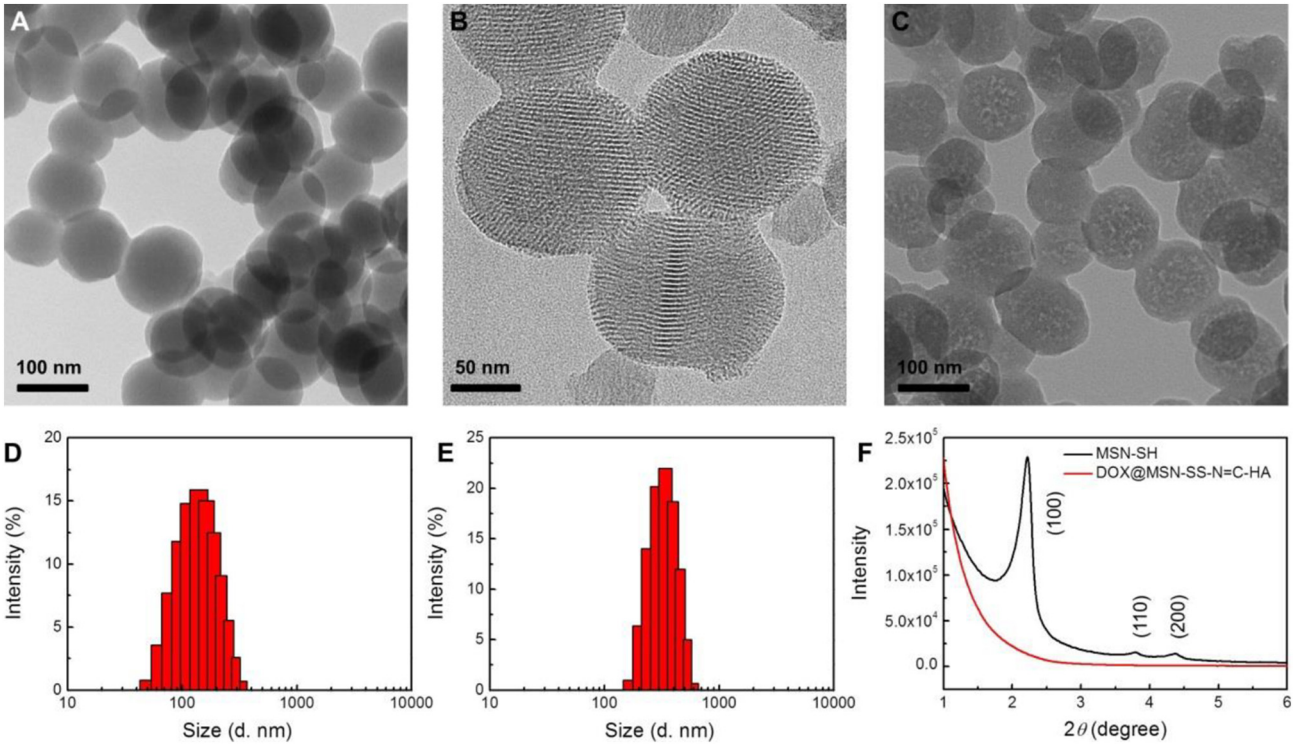

Fig. 2. TEM images of MSN-SH (A and B) and DOX@MSN-SS-N=C-HA (C); size distributions of MSN-SH (D) and DOX@MSN-SS-N=C-HA (E); and SAX patterns of MSN-SH and DOX@MSN-SS-N=C-HA (F).

the stretching vibration of N—H. And the stretching vibration of –SH at ~2563 cm^{-1} existed in the spectrum of MSN-SH (Fig. 4A) disappeared as well. The results proved the successful preparation of MSN-SS-NH_2. For MSN-SS-N=C-Ph, the weak characteristic absorption band of benzene skeleton vibration at ~1497 cm^{-1}, stretching vibration of C=N at ~1651 cm^{-1} and the disappearance of the characteristic absorption peak of the amino group demonstrated that –NH_2 of MSN-SS-NH_2 had been completely reacted into benzoic imine bond (Fig. 4C). The FT-IR spectrum of DOX@MSN-SS-N=C-HA was shown in Fig. 4D. New peaks of alkyl groups in both HA and β-CD-HN_2 at around 2910 to 2990 cm^{-1} as well as numerous apparent peaks of sugar ring in both HA and β-CD form 700 to 1600 cm^{-1} appeared in the spectrum, proved the successful preparation of the carriers.

TGA curves of MSN-SH, MSN-SS-NH_2, MSN-SS-N=C-Ph and the blank DDS MSN-SS-N=C-HA (without DOX) are shown in Fig. 5. With the carrying on of the surface modifications step by step, the weight loss values of the nanoparticles continuous rise. At 800 °C, the temperature decomposing the organic components completely, the weight loss values of the samples listed above were ~19.6%, 24.0%, 26.0% and 38.8%, respectively. The thermal weight loss of MSN-SH attributed to the organic components introduced by MPTMS, which were –C–SH (starting from ~260 °C) and alkyl (starting from ~400 °C). For MSN-SS-NH_2, the disulfide bond introduced led to the thermal weight loss at a lower temperature (~190 °C). And compared with MSN-SH, more organic components contained resulted in more weight loss. Further surface modification caused more weight loss of MSN-SS-N=C-Ph at 800 °C. And it could also be calculated from the TGA curves that for MSN-SS-N=C-HA, ~17.3 wt% of the carriers was HA-*g*-CD. The results could further demonstrate the successful surface modification of the nanoparticles.

3.2. Stability of DOX@MSN-SS-N=C-HA

It is expected that the drug carriers should have good stability during the circulation. As a result, the stability of DOX@MSN-SS-N=C-HA was investigated, as shown in Fig. 6. The carriers were dipped and shaken in RPMI-1640 medium with 10% FBS at 37 °C for 48 h. And the size of the nanoparticles was measured by DLS at a regular time. The size of the nanoparticles increased a little form ~365 nm tested in DI water to ~382 nm in RPMI-1640 medium with 10% FBS. However, the particle sizes could still keep in the range of around 382–424 nm during the testing time, proved the carriers were stable in RPMI-1640 medium with 10% FBS.

3.3. In vitro drug release studies

Due to the dual-responsive property of the carriers, the *in vitro* drug release studies were taken at different pH values with or without GSH (10 mM). The drug entrapment efficiency (*EE*) and drug loading capacity (*LC*) of DOX@MSN-SS-N=C-HA were measured to be 12.6% and 63.0%, respectively. As shown in Fig. 7, the drug release rate at pH 7.4 without GSH was quite slow. <10% of DOX was released form DOX@MSN-SS-N=C-HA within 8 h. And only ~17.7% of DOX was released within 72 h. At pH 6.5 without GSH, circumstance of tumor tissue, the drug release rate increased. However, the acceleration of the release rate still limited. The accumulative drug release amounts were ~17.0% and 31.4% within 8 and 72 h, respectively. The results suggest that DOX@MSN-SS-N=C-HA could effectively accommodate DOX before entering cancer cells, preventing premature drug release. Once being cellular uptake by cancer cells, the carriers should burst release the drugs intracellular. The conclusion could be demonstrated by the results of *in vitro* drug release studies at lower pH and the presence of GSH. It is noticed in Fig. 7 that when pH further reduced to 5.0, mimicking lysosome [43], the hydrolysis of benzoic imine bond led to the significant increase of the drug release rate. In buffer solution at pH 5.0 without GSH, about 17.8% of DOX was released within 2 h, which approached the accumulative drug release amount of DOX@MSN-SS-N=C-HA within 72 h at pH 7.4. And the drug release amounts increased to ~31.3% and 67.9% within 8 and 72 h, respectively.

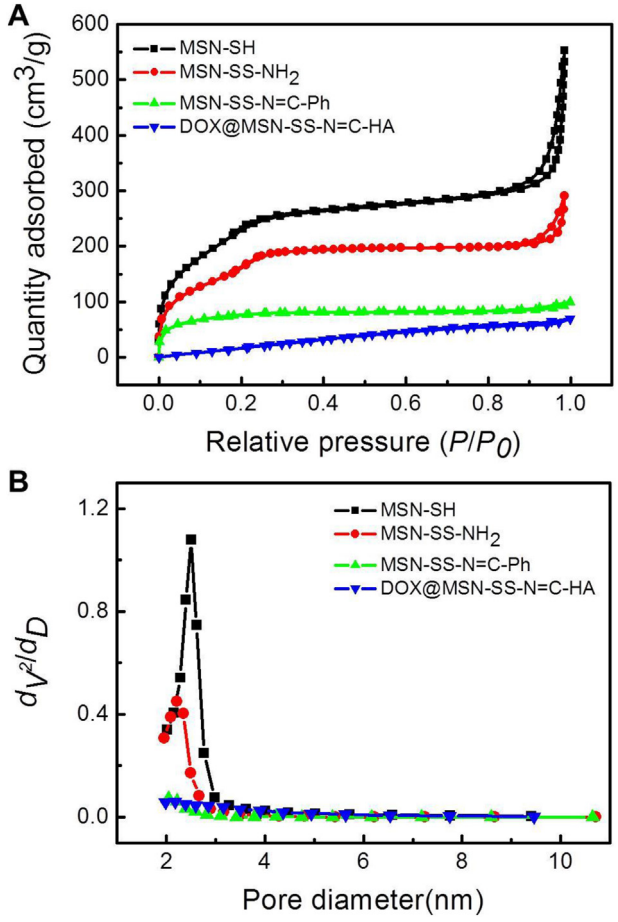

Fig. 3. Nitrogen adsorption–desorption isotherms (A) and BJH pore distributions (B) of MSN-SH, MSN-SS-NH_2, MSN-SS-N=C-Ph and DOX@MSN-SS-N=C-HA.

A similar phenomenon could be observed when the GSH concentration raised from 0 to 10 mM, the GSH concentration intra the cancer cells [45]. Due to the cleavage of the disulfide bond, the accumulative drug release amounts of the carriers at pH 7.4 with the concentration of GSH 10 mM were 7.7%, 30.9% and 60.7% within 2, 8 and 72 h, respectively. Buffer solution at pH 5.0 with the concentration of GSH 10 mM was finally chosen to simulate the intracellular environment. No doubt the carriers displayed the highest drug release rate under this condition. More than 20% of the loaded DOX was burst released within 2 h, which rose to ~40.0% within 8 h and ~80.2% within 72 h. The results of the *in vitro* drug release studies suggested that DOX@MSN-SS-N=C-HA could intracellular release DOX with a high rate due to the low pH and high concentration of GSH as well as a much slower rate before it entering the cancer cells.

Table 1
S_{BET}, V_p, D_{BJH} and zeta-potentials of MSN-SH, MSN-SS-NH_2, MSN-SS-N=C-Ph and DOX@MSN-SS-N=C-HA.

Sample	S_{BET} (m^2/g)	V_p (cm^3/g)	D_{BJH} (nm)	Zeta-potential (mV)
MSN-SH	873	0.855	2.86	−28.8
MSN-SS-NH_2	567	0.450	2.83	+41.5
MSN-SS-N=C-Ph	323	0.190	2.52	−35.8
DOX@MSN-SS-N=C-HA	58.0	0.108	/	−25.3

The sizes of the drug released DOX@MSN-SS-N=C-HA under different conditions were also measured. The size of the nanoparticles incubation in buffer solution at pH 5.0 without GSH for 72 h reduced to ~227 nm with a PDI of 0.152. And for buffer solution at pH 7.4 with 10 mM GSH and buffer solution at pH 5.0 with 10 mM GSH, the particle sizes were ~212 nm with a PDI of 0.147 and ~169 nm with a PDI of 0.207, respectively. It is believed that the acidic/redox environments could lead to the leaving of HA-*g*-CD, and resulted in the reducing of the particle size.

3.4. In vitro targeting analysis

The targeting ability of DOX@MSN-SS-N=C-HA against CD44 overexpressed cancer cells is one of the major factors for efficient cellular uptake of the carriers, which is a key requirement for the therapeutic efficacy. In this work, 4T1 ($CD44^+$) and 293T ($CD44^-$) cell lines were applied to investigate the targeting ability of the carriers by both CLSM and flow cytometry analysis. Before the analysis, carriers with green fluorescence based on FITC-modified MSN were prepared (DOX@MSN-SS-N=C-HA*). Fig. 8 shows the CLSM images of 4T1 and 293T cells *co*-incubation with DOX@MSN-SS-N=C-HA*. It is noticed that strong red fluorescence induced by DOX and green fluorescence induced by FITC appeared inside CD44 positive 4T1 cells (Fig. 8A–D), whereas a much weaker signal was observed in CD44 negative 293T cells (Fig. 8I–L). The quantitative results of flow cytometry analysis shown in Fig. 9 also indicated that the mean fluorescence intensity (MFI) value of both red fluorescence (1074, with the blank control of 171) and green fluorescence (5280, with the blank control of 368) in 4T1 cells was much stronger than that in 293T cells (823 for red fluorescence, with the blank control of 24; 1578 for green fluorescence, with the blank control of 51), proved that the cellular uptake ability of the carriers by 4T1 cells was evidently higher than that by 293T cells.

To further investigate the HA-based targeting ability, both cell lines were pretreated with free HA (5 mg/mL) to block the CD44-mediated pathway before they *co*-incubation with DOX@MSN-SS-N=C-HA*. As shown in Fig. 8E–H, after the pretreatment with HA, both red and green fluorescence inside 4T1 cells reduced significantly. The MFI

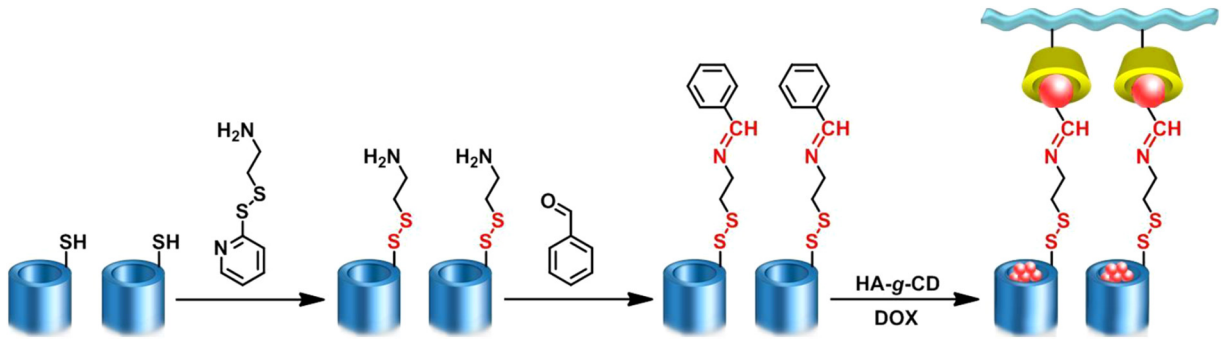

Scheme 1. Fabrication rout of DOX@MSN-SS-N=C-HA.

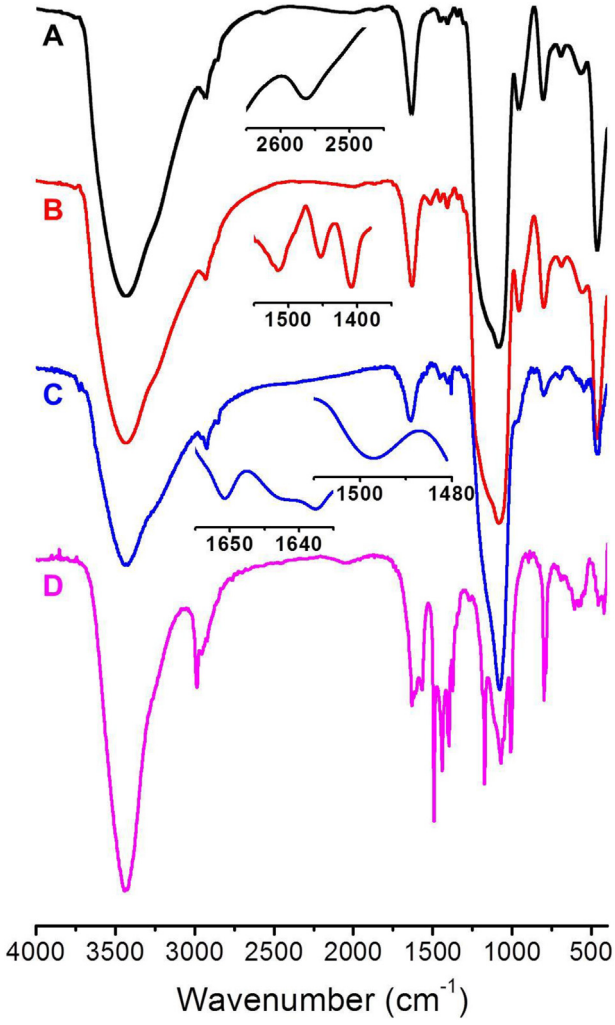

Fig. 4. FT-IR spectra of MSN-SH (A), MSN-SS-NH_2 (B), MSN-SS-N=C-Ph (C) and DOX@MSN-SS-N=C-HA (D).

value of red fluorescence reduced to ~0.77 fold of that without pretreatment, and the MFI value of green fluorescence reduced as well. The result suggested that due to the blocking of the CD44-mediated pathway could reduce the cellular uptake ability of DOX@MSN-SS-N=C-HA by

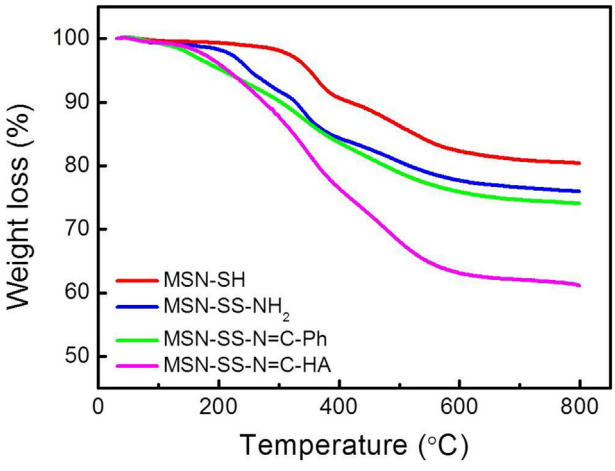

Fig. 5. TGA curves of MSN-SH, MSN-SS-NH_2, MSN-SS-N=C-Ph and MSN-SS-N=C-HA.

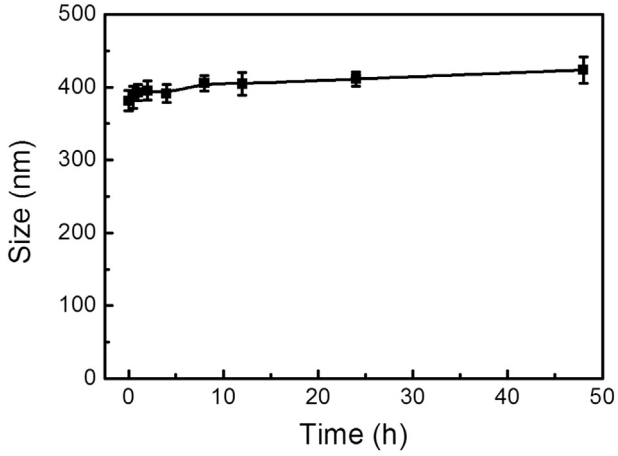

Fig. 6. Size change of DOX@MSN-SS-N=C-HA being dipped and shaken in RPMI-1640 medium with 10% FBS at 37 °C.

4T1 cells. In contrast, for the CD44 negative 293T cells there was no clear difference between the cells with and without pretreatment in the intensity of red fluorescence. Both the CLSM images (Fig. 8M–P) and the result of flow cytometry analysis (Fig. 9H) showed that the fluorescence intensity reduced little. All the data shown in both Figs. 8 and 9 proved the CD44-receptor mediated cancer cell targeting ability of the carriers.

3.5. In vitro cytotoxicity assay

4T1 and 293T cell lines were introduced for the *in vitro* cytotoxicity studies as well. As shown in Fig. 10A and C, the cytotoxicity of blank DDS (MSN-SS-N=C-HA, with no DOX loaded) was low. For 4T1 cells, the cell viability at the concentration of MSN-SS-N=C-HA 3.2 mg/L was ~93.5%. With the concentration of the blank carriers raised to 25 and 100 mg/L, the cell viabilities were still above 85% and 81%, respectively. For 293T cells, the cell viability kept above 82% with the concentration of the blank carriers raised from 0.78 to 25 mg/L. And the cell viability was ~73.7% at the concentration of MSN-SS-N=C-HA 100 mg/L. The results proved the blank carriers without loading of DOX had low cytotoxicity and were suitable for the *in vitro* cellular study.

The results in the *in vitro* targeting analysis demonstrated that the CD44-receptor mediated cancer cell targeting ability of DOX@MSN-SS-

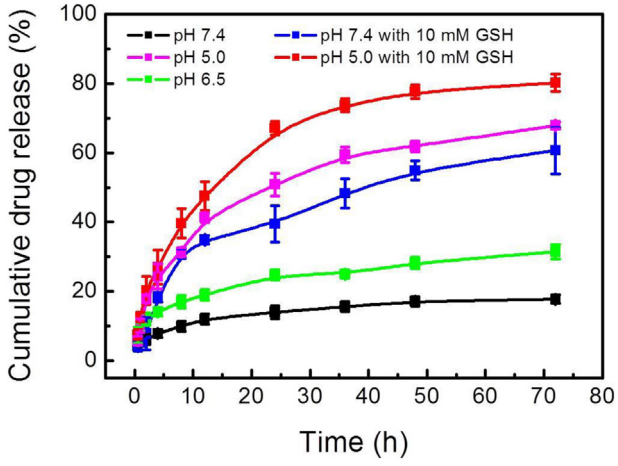

Fig. 7. The controlled release profiles of DOX@MSN-SS-N=C-HA at different pH values (7.4, 6.5 and 5.0) and different concentrations of GSH (0 and 10 mM).

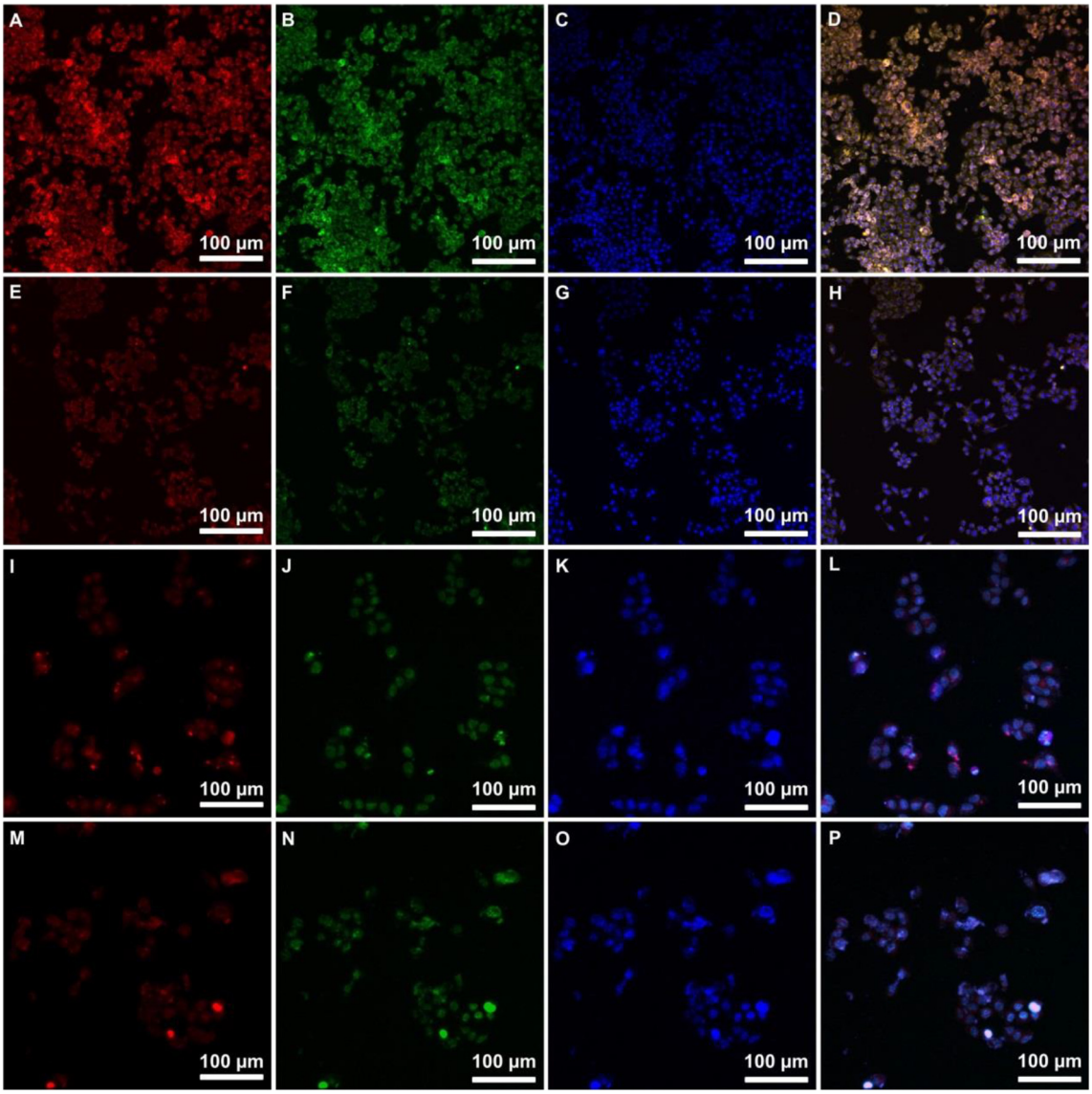

Fig. 8. CLSM images of 4T1 (A–H) and 293T (I–P) cells incubated with DOX@MSN-SS-N=C-HA*: (A, E, I and M) red fluorescence induced from DOX, (B, F, J and N) green fluorescence induced from FITC, (C, G, K and O) blue fluorescence induced from DAPI indicating of nucleus and (D, H, L and P) an overall of red, green and blue fluorescence. E–H and M–P: cells pretreated with 5 mg/mL of free HA. (For interpretation of the references to colour in this figure legend, the reader is referred to the web version of this article.)

N=C-HA played an important role in the cellular uptake of the carriers. That is, the cellular uptake of the carriers by CD44 receptor over-expressed 4T1 cells was much easier than that of 293T cells. And the results of the *in vitro* cytotoxicity assay also met the conclusion. As shown in Fig. 10B, DOX@MSN-SS-N=C-HA exhibited a strong capability for 4T1 cell apoptosis, which was slightly lower than that of free DOX. After being *co*-incubated with the carriers for 48 h, the cell viability of 4T1 cells decreased to ~52.4% at the DOX concentration of 0.32 mg/L, and kept decreasing to ~24.7% and 13.4% at the DOX concentrations of 2.5 and 10 mg/L, respectively. By contrast, the cell viabilities of 4T1 cells *co*-incubated with free DOX were ~52.1%, 23.7% and 8.6% at the concentrations of 0.32, 2.5 and 10 mg/L, respectively. However, for the CD44 negative 293T cells, as shown in Fig. 10D, after being *co*-incubated with the carriers for 48 h the cell viabilities of were ~67.7%, 42.4% and 36.6% at the DOX concentrations of 0.32, 2.5 and 10 mg/L respectively, which were much higher than that of free DOX (~50.0%, 21.9% and 11.2% at the concentrations of 0.32, 2.5 and 10 mg/L, respectively).

To further investigate the targeting ability of DOX@MSN-SS-N=C-HA, both 4T1 and 293T cells were also pretreated with free HA before the cytotoxicity studies. As shown in Fig. 10B and D, the changes in cell viability were quite different for both cell lines. Only ~29.7%, 56.1% and 68.7% of 4T1 cells were killed at the DOX concentrations of 0.32, 2.5 and 10 mg/L respectively, which were significantly lower than that of 4T1 cells without pretreatment. Blocking of the CD44-mediated pathway by free HA could decrease the amount of endocytosis of the carriers, leading to the obviously increasing of the cell viability. For 293T cells the cell viability changed few (~74.5%, 46.8% and 38.2% at the DOX concentrations of 0.32, 2.5 and 10 mg/L, respectively). The IC_{50} values calculated from MTT studies are shown in Table 2. And the data also shown the obvious differences between the cytotoxicity of DOX@MSN-SS-N=C-HA in both cell lines with or without pretreated with free HA. The results further proved the targeted cancer therapy capability of DOX@MSN-SS-N=C-HA.

4T1 cells were also pretreated with NH_4Cl, BSO and both NH_4Cl and BSO, respectively. NH_4Cl can trigger the restoration of intracellular pH [50,51]; therefore, as shown in Fig. 11, after being *co*-incubated with DOX@MSN-SS-N=C-HA for 48 h, the cell viability of 4T1 cells pretreated with 20 mM NH_4Cl increased. The cell viabilities at the DOX concentrations of 0.32, 2.5 and 10 mg/L were ~65.4%, 29.2% and

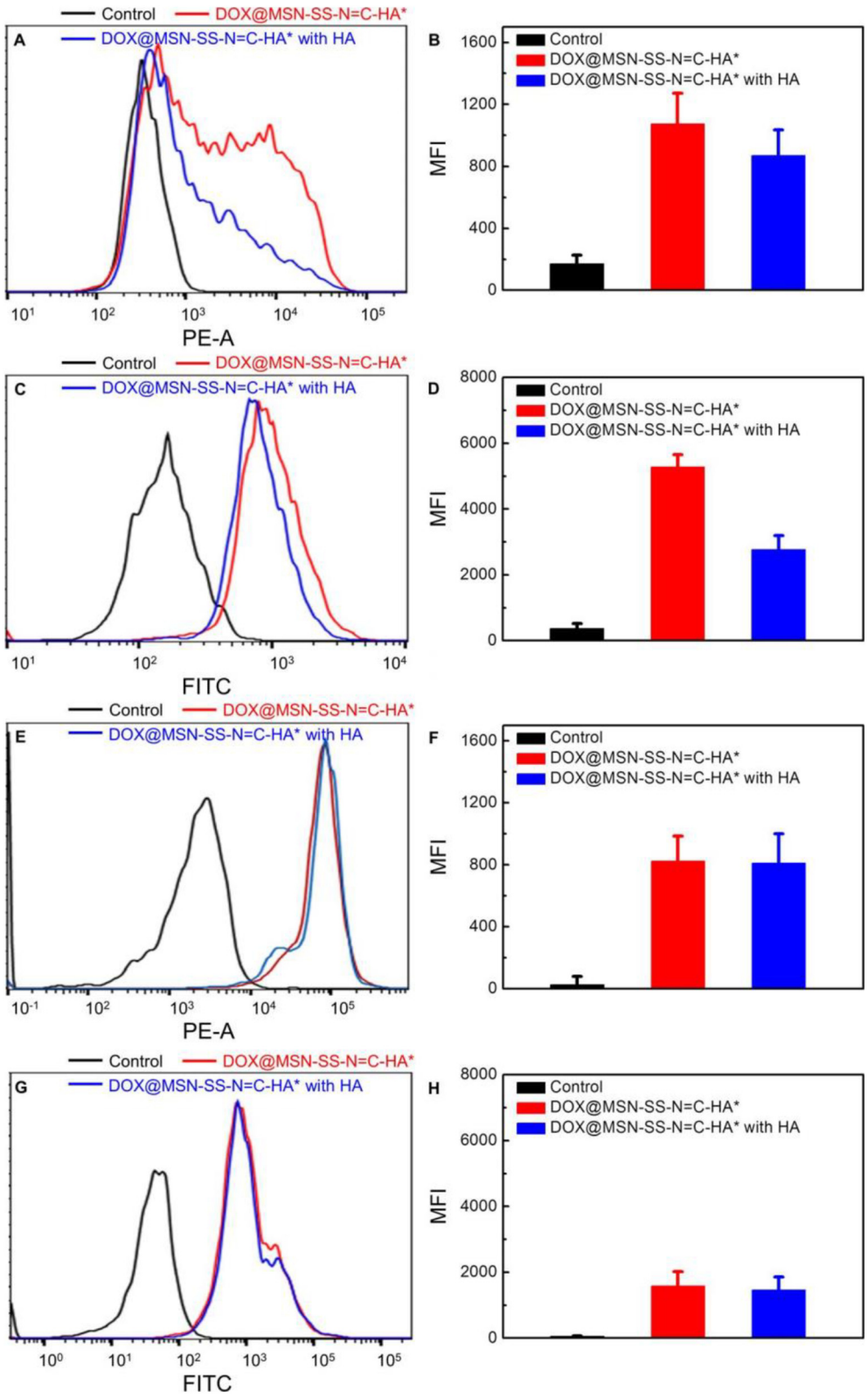

Fig. 9. Flow cytometry analyses of 4T1 (A–D) and 293T (E–H) cells incubated with DOX@MSN-SS-N=C-HA* for 4 h without (red) and with (blue) free HA pretreatment. Blank was used as a control (black). The concentration of DOX was 4 mg/L. (For interpretation of the references to colour in this figure legend, the reader is referred to the web version of this article.)

17.7% respectively, much higher than that without pretreatment. The higher pH caused a slower drug release rate of the carriers intracellular, which led to the higher cell viability. BSO is a specific γ-glutamylcysteine synthetase inhibitor that blocks the rate-limiting step of glutathione biosynthesis and can reduce GSH level intracellular [51]. As a result, similar to that of 4T1 cells pretreated with NH_4Cl, cell viability of 4T1 cells pretreated with 500 μm BSO increased as well (~61.3%, 25.2% and 15.9% at the DOX concentrations of 0.32, 2.5 and

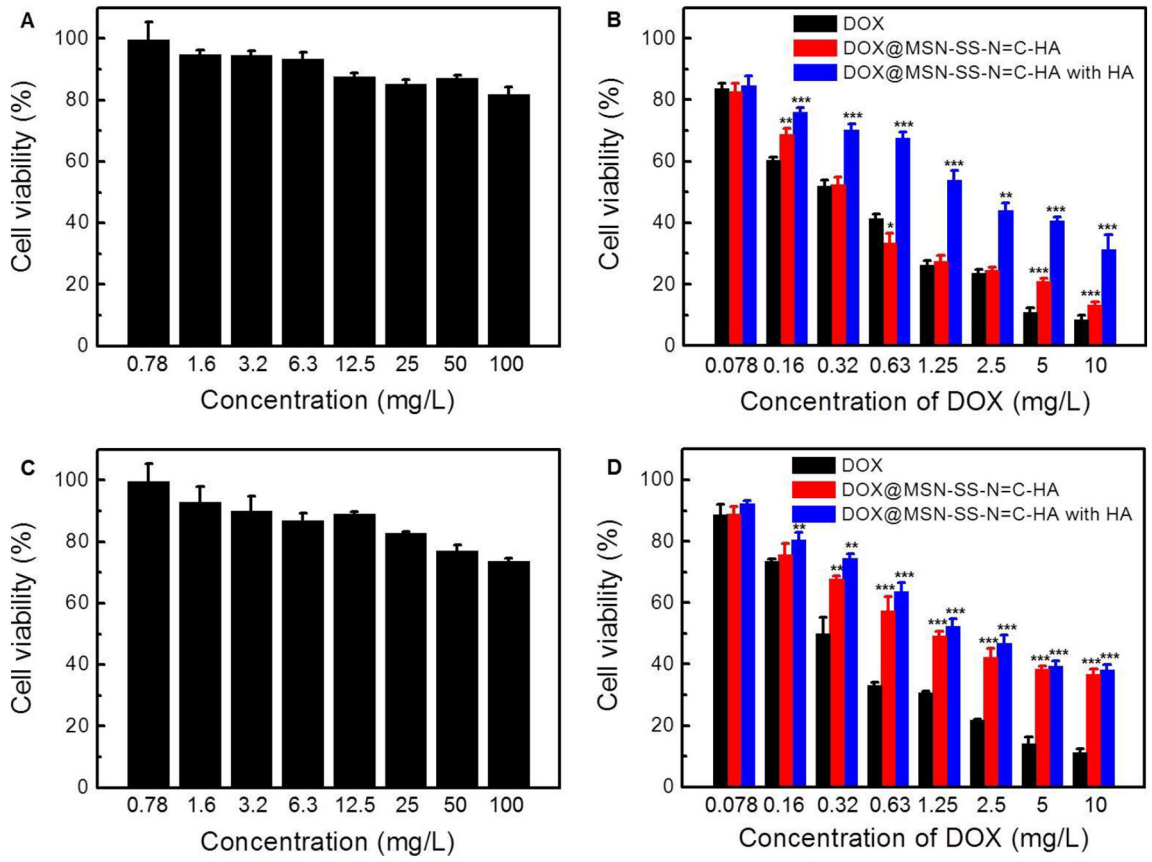

Fig. 10. Cell viability of 4T1 (A) and 293T (C) cells incubated with MSN-SS-N=C-HA with different concentrations, and 4T1 (B) and 293T (D) cells incubated with DOX@MSN-SS-N=C-HA with different DOX concentrations. The cells were pretreated with free HA and not pretreated, respectively. Statistical significance in differences was analyzed compared to the cell viability of free DOX.

10 mg/L, respectively). For 4T1 cells pretreated with both NH_4Cl and BSO, the cell viability further increased. Only ~33.1%, 70.0% and 81.9% of cells were killed at the DOX concentrations of 0.32, 2.5 and 10 mg/L respectively. The results further proved the dual-responsiveness of DOX@MSN-SS-N=C-HA.

4. Conclusions

In conclusion, based on host-guest interaction, a dual-responsive targeting DDS named DOX@MSN-SS-N=C-HA was prepared for cancer therapy. MSN, which was modified with benzene ring through both pH-sensitive benzoic imine bond and redox-sensitive disulfide bond, was utilized to load the chemotherapeutic drug DOX. Then the nanoparticles were capped by HA-*g*-CD through host-guest interaction between β-CD and benzene. Thanks to HA, the carriers were CD44 over-expressed cancer cell targeted. And after the carriers entering the cancer cells, the acidic environment, as well as the high concentration of GSH, could lead to the left of the "gatekeeper", resulting in controlled DOX release intracellular. The carriers showed an excellently targeted cancer

Table 2
IC_{50} values (mg/L) of DOX and DOX@MSN-SS-N=C-HA in different cell lines.

Sample	IC_{50}	
	4T1	293T
DOX	0.072	0.120
DOX@MSN-SS-N=C-HA	0.208	0.324
DOX@MSN-SS-N=C-HA with HA	1.25	0.388
DOX@MSN-SS-N=C-HA with NH_4Cl	0.312	/
DOX@MSN-SS-N=C-HA with BSO	0.362	/
DOX@MSN-SS-N=C-HA with NH_4Cl and BSO	0.375	/

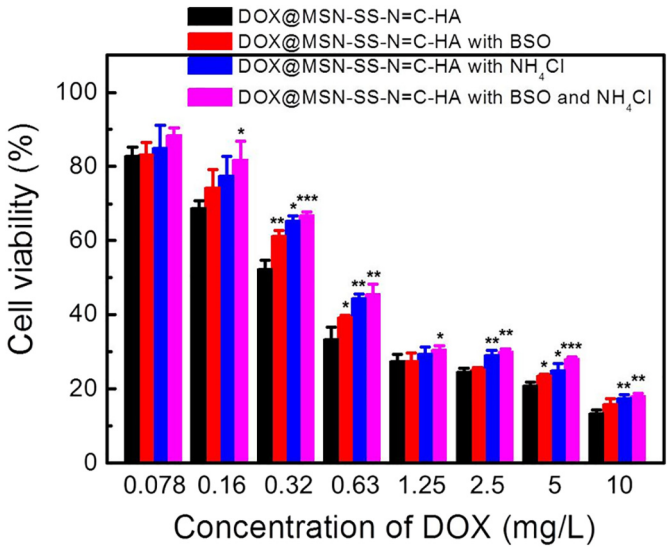

Fig. 11. Cell viability of 4T1 cells incubated with DOX@MSN-SS-N=C-HA with different DOX concentrations. The 4T1 cells were pretreated with NH_4Cl, pretreated with BSO, pretreated with both NH_4Cl and BSO and not pretreated, respectively. Statistical significance in differences was analyzed compared to the cell viability without pretreatment.

therapy capability *in vitro* and could provide new ideas for the design of targeting anti-cancer DDSs.

CRediT authorship contribution statement

Jinbo Lu: Investigation, Writing - original draft. **Bichu Luo:** Investigation, Writing - original draft. **Zhongyin Chen:** Investigation. **Ye Yuan:** Investigation. **Ying Kuang:** Formal analysis. **Lihui Wan:** Investigation. **Li Yao:** Funding acquisition. **Xueqin Chen:** Writing - review & editing. **Bingbing Jiang:** Writing - review & editing. **Jia Liu:** Methodology. **Cao Li:** Funding acquisition, Methodology, Writing - review & editing.

Acknowledgements

This study was funded by National Natural Science Foundation of China (51773055, 51503060 and 51503059) and Wuhan Morning Light Plan of Youth Science and Technology (2017050304010283).

References

[1] T.M. Allen, P.R. Cullis, Science 303 (2004) 1818–1822.
[2] H. Chen, Z. Gu, H. An, C. Chen, J. Chen, R. Cui, S. Chen, W. Chen, X. Chen, X. Chen, Z. Chen, B. Ding, Q. Dong, Q. Fan, T. Fu, D. Hou, Q. Jiang, H. Ke, X. Jiang, G. Liu, S. Li, T. Li, Z. Liu, G. Nie, M. Ovais, D. Pang, N. Qiu, Y. Shen, H. Tian, C. Wang, H. Wang, Z. Wang, H. Xu, J.F. Xu, X. Yang, S. Zhu, X. Zheng, X. Zhang, Y. Zhao, W. Tan, X. Zhang, Y. Zhao, Sci. China Chem. 61 (2018) 1503–1552.
[3] J. Shi, P.W. Kantoff, R. Wooster, O.C. Farokhzad, Nat. Rev. Cancer 17 (2017) 20–37.
[4] O.S. Fenton, K.N. Olafson, P.S. Pillai, M.J. Mitchell, R. Langer, Adv. Mater. 30 (2018), 1705328.
[5] S.K. Golombek, J.N. May, B. Theek, L. Appold, N. Drude, F. Kiessling, T. Lammers, Adv. Drug Deliver. Rev. 130 (2018) 17–38.
[6] Q. Sun, X. Sun, X. Ma, Z. Zhou, E. Jin, B. Zhang, Y. Shen, E.A. Van Kirk, W.J. Murdoch, J.R. Lott, T.P. Lodge, M. Radosz, Y. Zhao, Adv. Mater. 26 (2014) 7615–7621.
[7] Q. Sun, Z. Zhou, N. Qiu, Y. Shen, Adv. Mater. 29 (2017) 1606628.
[8] D.L. Stirland, J.W. Nichols, S. Miura, Y.H. Bae, J. Control. Release 172 (2013) 1045–1064.
[9] H. Cabral, K. Kataoka, J. Control. Release 190 (2014) 465–476.
[10] Y. Lu, A.A. Aimetti, R. Langer, Z. Gu, Nat. Rev. Mater. 2 (2016), 16075.
[11] F. Seidi, R. Jenjob, D. Crespy, Chem. Rev. 118 (2018) 3965–4036.
[12] T. Ojha, V. Pathak, Y. Shi, W.E. Hennink, C.T.W. Moonen, G. Storm, F. Kiessling, T. Lammers, Adv. Drug Deliver. Rev. 119 (2017) 44–60.
[13] N. Bertrand, J. Wu, X. Xu, N. Kamaly, O.C. Farokhzad, Adv. Drug Deliver. Rev. 66 (2014) 2–25.
[14] D. Dheer, D. Arora, S. Jaglan, R.K. Rawal, R. Shankar, J. Drug Target. 25 (2017) 1–16.
[15] S.Y. Qin, A.Q. Zhang, X.Z. Zhang, Small 14 (2018) 1802417.
[16] J. Wen, K. Yang, F. Liu, H. Li, Y. Xu, S. Sun, Chem. Soc. Rev. 46 (2017) 6024–6045.
[17] T. Li, S. Shi, S. Goel, X. Shen, X. Xie, Z. Chen, H. Zhang, S. Li, X. Qin, H. Yang, C. Wu, Y. Liu, Acta Biomater. 89 (2019) 1–13.
[18] J.G. Croissant, Y. Fatieiev, A. Almalik, N.M. Khashab, Adv. Healthcare Mater. 7 (2018) 1700831.
[19] E. Aznar, M. Oroval, L. Pascual, J.R. Murguía, R. Martínez-Máñez, F. Sancenón, Chem. Rev. 11 (2016) 561–62718.
[20] P. Bilalis, L.A. Tziveleka, S. Varlasa, H. Iatrou, Polym. Chem. 7 (2016) 1475–1485.
[21] M. Zhang, J. Liu, Y. Kuang, Q. Li, D.W. Zheng, Q. Song, H. Chen, X. Chen, Y. Xu, C. Li, B. Jiang, Int. J. Biol. Macromol. 98 (2017) 691–700.
[22] S. Baek, R.K. Singh, T.H. Kim, J.W. Seo, U.S. Shin, W. Chrzanowski, H.W. Kim, ACS Appl. Mater. Interfaces 8 (2016) 8967–8979.
[23] F. Yu, H. Wu, Y. Tang, Y. Xu, X. Qian, W. Zhu, Int. J. Pharm. 536 (2018) 11–20.
[24] Y. Jiao, Y. Sun, B. Chang, D. Lu, W. Yang, Chem. Eur. J. 19 (2013) 15410–15420.
[25] M. Zhang, J. Liu, Y. Kuang, Q. Li, H. Chen, H. Ye, L. Guo, Y. Xu, X. Chen, C. Li, B. Jiang, J. Mater. Chem. B 4 (2016) 3387–3397.
[26] J. Liu, B. Chang, Q. Li, L. Xu, X. Liu, G. Wang, Z. Wang, L. Wang, Adv. Sci. 6 (2019) 1801987.
[27] L. Qiu, W. Zhang, S. Wang, X. Zhang, Y. Zhao, L. Cao, L. Sun, Mater. Sci. Eng. C Mater. Biol. Appl. 81 (2017) 485–491.
[28] C. Yang, W. Guo, N. An, L. Cui, T. Zhang, R. Tong, Y. Chen, H. Lin, F. Qu, RSC Adv. 5 (2015) 80728–80738.
[29] G. Wang, J. Dong, T. Yuan, J. Zhang, L. Wang, H. Wang, Macromol. Biosci. 16 (2016) 990–994.
[30] J. Zhang, D. Wu, M.F. Li, J. Feng, ACS Appl. Mater. Interfaces 7 (2015) 26666–26673.
[31] C. Chen, W. Yao, W. Sun, T. Guo, H. Lv, X. Wang, H. Ying, Y. Wang, P. Wang, Int. J. Biol. Macromol. 122 (2019) 1090–1099.
[32] S. Tiwari, P. Bahadur, Int. J. Biol. Macromol. 121 (2019) 556–571.
[33] K.Y. Choi, H.S. Han, E.S. Lee, J.M. Shin, B.D. Almquist, D.S. Lee, J.H. Park, Adv. Mater. 31 (2019) 1803549.
[34] H. Knopf-Marques, M. Pravda, L. Wolfova, V. Velebny, P. Schaaf, N.E. Vrana, P. Lavalle, Adv. Healthcare Mater. 5 (2016) 2841–2855.
[35] Z. Chen, Z. Li, Y. Lin, M. Yin, J. Ren, X. Qu, Chem. Eur. J. 19 (2013) 1778–1783.
[36] M. Yu, S. Jambhrunkar, P. Thorn, J. Chen, W. Gu, C. Yu, Nanoscale 5 (2013) 178–183.
[37] Q. Zhao, H. Geng, Y. Wang, Y. Gao, J. Huang, Y. Wang, J. Zhang, S. Wang, ACS Appl. Mater. Interfaces 6 (2014) 20290–20299.
[38] Q. Zhao, J. Liu, W. Zhu, C. Sun, D. Di, Y. Zhang, P. Wang, Z. Wang, S. Wang, Acta Biomater. 23 (2015) 147–156.
[39] J. Zhang, Y. Sun, B. Tian, K. Li, L. Wang, Y. Liang, J. Han, Colloids Surf. B 144 (2016) 293–302.
[40] J. Ding, T. Liang, Y. Zhou, Z. He, Q. Min, L. Jiang, J. Zhu, Nano Res. 10 (2017) 690–703.
[41] L. Huang, J. Liu, F. Gao, Q. Cheng, B. Lu, H. Zheng, H. Xu, P. Xu, X. Zhang, X. Zeng, J. Mater. Chem. B 6 (2018) 4618–4629.
[42] V. Nairi, S. Magnolia, M. Piludu, M. Nieddu, C.A. Caria, V. Sogos, M. Vallet-Regì, M. Monduzzi, A. Salis, Colloids Surf. B 168 (2018) 50–59.
[43] R. Mo, Z. Gu, Mater. Today 19 (2016) 274–283.
[44] M. Kanamala, W.R. Wilson, M. Yang, B.D. Palmer, Z. Wu, Biomaterials 85 (2016) 152–167.
[45] S. Chakravarthi, C.E. Jessop, N.J. Bulleid, EMBO Rep. 7 (2006) 271–275.
[46] H. Sun, Y. Zhang, Z. Zhong, Adv. Drug Deliver. Rev. 132 (2018) 16–32.
[47] H. Chen, Z. Chen, Y. Kuang, S. Li, M. Zhang, J. Liu, Z. Sun, B. Jiang, X. Chen, C. Li, Colloids Surf. B 167 (2018) 407–414.
[48] Y.W. Ebright, Y. Chen, Y. Kim, R.H. Ebright, Bioconjug. Chem. 7 (1996) 380–384.
[49] Z.Y. Li, J.J. Hu, Q. Xu, S. Chen, H.Z. Jia, Y.X. Sun, R.X. Zhuo, X.Z. Zhang, J. Mater. Chem. B 3 (2015) 39–44.
[50] H. Chen, Y. Kuang, R. Liu, Z. Chen, B. Jiang, Z. Sun, X. Chen, C. Li, J. Mater. Sci. 53 (2018) 10653–10665.
[51] J. Liu, X. Liu, Y. Yuan, Q. Li, B. Chang, L. Xu, B. Cai, C. Qi, C. Li, X. Jiang, G. Wang, Z. Wang, L. Wang, ACS Appl. Mater. Interfaces 10 (2018) 26473–26484.